BIOCHEMISTRY
including biophysical chemistry & molecular biology

Article

pubs.acs.org/biochemistry

Role of Polarity of the Distal Pocket in the Control of Inhibitor Binding in Dehaloperoxidase-Hemoglobin

Ashlee Plummer,[†] Matthew K. Thompson,[‡] and Stefan Franzen*,[†]

[†]Department of Chemistry, North Carolina State University, Raleigh, North Carolina 27695, United States

[‡]Department of Biochemistry, Vanderbilt University Medical Center, Nashville, Tennessee 37232, United States

Supporting Information

ABSTRACT: Dehaloperoxidase (DHP A), a unique multifunctional enzyme, from the marine annelid *Amphitrite ornata* dehalogenates 2,4,6-tribromophenol to form 2,6-dibromo-1,4-benzoquinone. The catalytic cycle of DHP is similar to that of horseradish peroxidase (HRP), involving a high-valent ferryl heme and two single-electron transfers from the aromatic substrate to the enzyme. Like HRP, DHP has been investigated as a potential bioremediation enzyme. However, DHP fails as a bioremediation enzyme because, unlike HRP, it has an internal binding cavity on the distal side of the heme capable of accommodating *p*-bromophenols, which act as an inhibitor of peroxidase function. Blocking internal binding in DHP may be the key to allowing the enzyme to function effectively as a peroxidase on the full range of halogenated phenols. The distal cavity of DHP is surrounded by several hydrophobic amino acids that stabilize internal binding of the monohalogenated phenols, including a leucine residue near the back edge of the heme (L100). We have expressed the L100F, L100Q, L100T, and L100V mutants of DHP in an effort to prevent internal binding and thereby convert the inhibitors into substrates. Kinetic assays and resonance Raman indicate that the peroxidase activity of the L100T and L100F mutants is increased compared to that of native DHP in the presence of 4-bromophenol (4-BP), suggesting a reduction in the inhibitor binding constant. In addition, the X-ray crystal structure of L100F clearly indicates a reduced occupancy of the 4-BP inhibitor in the distal cavity of DHP. However, at the same time, the L100F structure reveals that steric interference alone is insufficient to exclude the inhibitor. Instead, the comparison of L100T and isosteric L100V reveals that an increase in polarity plays a decisive role in excluding the inhibitor from the distal binding pocket.

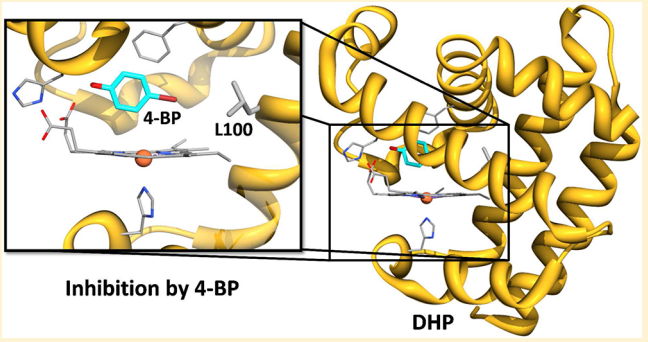

The enzyme dehaloperoxidase-hemoglobin (DHP) was first isolated from the terebellid polychaete *Amphitrite ornata* and is a heme-containing peroxidase that also functions as a globin.[1] In a manner similar to that of horseradish peroxidase (HRP),[2] DHP dehalogenates 2,4,6-tribromophenol (2,4,6-TBP) and other trihalophenols in the presence of H_2O_2, as shown in Scheme 1.[1] DHP was first discovered as the hemoglobin of *A. ornata*[3] and therefore must have an important function in oxygen transport in addition to the subsequently discovered peroxidase function.[1] There are significant environmental implications of this naturally occurring peroxidase activity, as the toxicity of phenol derivatives has been proven both in vitro and in vivo. Government restrictions on the use of chlorinated phenol reagents are becoming increasingly stringent,[4−6] which provides motivation for the study of enzymes capable of degrading such compounds. While chlorinated compounds are predominantly produced by human industrial processes, brominated phenols are widespread in coastal ecosystems because of an abundance of marine organisms that produce these molecules as repellents or for other protective functions.[7] Ironically, *A. ornata* lacks the ability to produce brominated phenols, although it appears to have highly specific interactions with both 2,4,6-TBP and 4-bromophenol (4-BP).[8]

DHP exists as a crystallographic dimer but has recently been shown by small-angle X-ray scattering measurements to be mostly monomeric in solution.[9] There are two isoforms of DHP, known as DHP A and DHP B.[10] Given the extensive data available for DHP A relative to the data for the recently characterized DHP B,[11,12] the remainder of this study will focus

Scheme 1. Conversion of Trihalogenated Phenols into the Quinone Product by DHP A

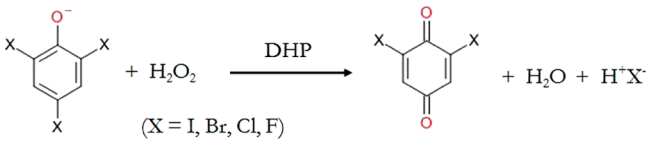

Received: November 7, 2012
Revised: March 8, 2013
Published: March 12, 2013

   dx.doi.org/10.1021/bi301509r | *Biochemistry* 2013, 52, 2218−2227

on DHP A, which will be termed DHP hereafter for the sake of brevity.[1,3,13,14]

DHP is classified as a globin based on X-ray crystal structures that show eight α-helices arranged in a fold that is unique to myoglobins and hemoglobins.[13,15,16] X-ray crystal structures, Fourier transform infrared, and nuclear magnetic resonance (NMR) have clearly established the existence of an internal binding site for 4-BP above the heme of DHP, a unique feature not found in other globins.[17−19] Internal binding of 4-BP results in inhibition of the peroxidase function of DHP.[8,20] The binding of an inhibitor in a well-defined internal binding pocket, combined with its unusually high peroxidase activity, indicates that DHP is not only a hemoglobin but also a protein that regulates the concentration of at least two toxins found in the coastal ecosystem inhabited by *A. ornata*.

We have shown previously that substrate oxidation of 2,4,6-TCP occurs at the heme edge via a radical mechanism, although the exact substrate binding site is unknown.[21] On the basis of extensive evidence, it has been proposed that DHP may possess an external binding site for substrate oxidation, in addition to the internal binding site recently observed by X-ray crystallography experiments.[8,17−19,22] It is important to note that the most frequently used substrate has been 2,4,6-trichlorophenol (2,4,6-TCP) because its solubility is greater than that of the native substrate, 2,4,6-tribromophenol. In addition, there is a precedent for studies of 2,4,6-TCP oxidation by HRP.[23,24] However, it is possible that 2,4,6-TCP and 2,4,6-TBP bind to DHP in a different manner. The surface binding, which is considered the norm in peroxidases, may be a special case for 2,4,6-TCP given that 2,4,6-TBP has a different kinetic profile and potentially different binding site.[25]

Although the exact substrate binding site is unknown, X-ray crystal structures have revealed the binding site of a nonclassical competitive inhibitor, 4-BP, in the heme cavity.[8,26] We use the term "nonclassical competitive inhibition" to refer to two-site competitive inhibition. X-ray crystallography experiments also revealed that the distal histidine (H55) plays a key role in the chemistry of the heme pocket of DHP by alternating between an open and closed conformation.[19,27] These two sites are defined relative to a similar set of conformations in sperm whale myoglobin (SWMb)[28,29] in which the distal histidine can be either in the interior of the distal cavity in the proximity of diatomic ligands (such as O_2) bound to the heme Fe (closed) or in a solvent-exposed conformation pointing away from the heme Fe (open). The conformational flexibility of H55 in DHP appears to be greater than in other globins based on the X-ray crystal structures.[15,16,27] X-ray crystal structures of DHP show that in the presence of a monohalogenated inhibitor, the distal H55 is pushed into the open conformation.[13,15,19] The conformational change from closed to open inhibits DHP from oxidizing 2,4,6-TBP to form 2,6-DBQ. The inhibition is due in part to the competition between inhibitor and substrate binding, which we have previously shown to be mediated by H55,[8,17,20] and in part to the fact that the inhibitor blocks the heme Fe and therefore impedes the binding of H_2O_2 to the enzyme active site.[8]

DHP has been shown to bind the inhibitor and a series of analogues, 4-iodophenol, 4-bromophenol, 4-chlorophenol, and 4-fluorophenol (4-IP, 4-BP, 4-CP, and 4-FP, respectively) with a trend in binding constants that decreases as the halogen size decreases: I > Br > Cl > F.[8] Thompson et al. suggest that the para-halogen atom of the 4-XP inhibitor determines the binding affinity of the inhibitor in the distal cavity. Additional studies of Xe-derivatized and inhibitor-bound X-ray crystal structures of DHP suggest that a Xe-binding site coincides with the para-bromine atom of the inhibitor 4-BP.[19] This evidence strongly suggests that steric control of inhibitor binding is prevalent in the distal heme cavity of DHP. Therefore, we suggest that altering the sterics of the distal heme cavity may affect the inhibitor binding constant of DHP by lowering its affinity for the inhibitor binding site. In an effort to determine the nature of the interaction of the inhibiting monohalogenated phenol with the heme cavity and its effect on enzyme function, site-directed mutagenesis at the L100 residue site in DHP has been studied. The selection of the L100 position for detailed study is based in part on the fact that this amino acid residue is situated in the 4-BP binding cavity; this target for the study of the determinants of internal binding was chosen after an extensive series of mutations not considered here. The L100 residue is approximately 4 Å from the bromine of the inhibitor molecule and 6 Å from the heme Fe. Mutations were chosen to vary the polarity and steric environment of the distal heme cavity, similar to the Phe41 mutations studied in horseradish peroxidase.[30] The importance of the L100 site was first suggested when NMR experiments showed that the L100 residue was shifted by substrate binding even though it is buried in the enzyme.[17] A role for L100 has also been suggested in a recent X-ray crystal structure designed to test the convergence of globin and peroxidase functions.[31] In this work, we report the characterization of the DHP mutants L100 → F100 (L100F), L100 → Q100 (L100Q), L100 → T100 (L100T), and L100 → V100 (L100V) by UV−vis kinetic assays, resonance Raman (RR), X-ray crystallography (L100F only), and molecular dynamics (MD) simulations. The results of this study further support the hypothesis that the internal binding of 4-BP is a unique feature of the dehaloperoxidase-hemoglobin. However, we will find that a simple steric picture does not account for the effect of the mutations at position L100.

MATERIALS AND METHODS

Mutagenesis. The mutagenesis reactions were performed using the QuikChange multi site-directed mutagenesis kit (Stratagene). DNA was purified from transformants using the QIAprep Spin Mini-prep kit (Qiagen, Valencia, CA). All mutations were verified by sequence analysis.

Mutant Protein Growth. The expression and purification of His_6-DHP has been discussed elsewhere.[32] We utilized a modified protocol, in which IPTG induction was not necessary because of a leaky promoter in the cell line, and the time for 6 L growths was lengthened to 15 h. pET-16b plasmids containing the His_6-tagged DHP L100F, L100T, L100V, and L100Q DNA inserts were transformed into competent BL21(DE3) *Escherichia coli* cells and then plated with 100 μg/mL ampicillin and allowed to grow at 37 °C for ∼14 h. Single colonies were isolated and transferred to 2 mL starter growths of 2×YT broth containing 80 μg/mL ampicillin at 37 °C with shaking for ∼8 h. A portion of the 1 mL of each starter growth was then used to inoculate six 1 L flasks of 2×YT broth containing 80 μg/mL ampicillin. The 6 L *E. coli* growth was incubated at 37 °C with shaking for ∼15 h. The cells were collected via centrifugation at 7000 rpm and 4 °C for 20 min.

Purification of His-Tagged Mutants. Each cell pellet was suspended in 100 mL of His tag lysis buffer [50 mM NaH_2PO_4, 300 mM NaCl, and 10 mM imidazole (pH 8)] and 200 mg of lysosome. The solution was stirred at 4 °C for 1 h; 100 μL of

dx.doi.org/10.1021/bi301509r | *Biochemistry* 2013, 52, 2218−2227

DNase and RNase were added to the solution, which was then stirred at 4 °C for 1 h. The resulting mixture was frozen overnight. It was then thawed and centrifuged at 17000 rpm for 30 min. The supernatant was collected and loaded on a Ni-NTA column. The column was then washed with washing buffer [50 mM NaH_2PO_4, 300 mM NaCl, and 50 mM imidazole (pH 8)]; the protein was eluted with elution buffer [50 mM NaH_2PO_4, 300 mM NaCl, and 250 mM imidazole (pH 8)]. The protein was then oxidized by the addition of excess potassium ferricyanide and loaded onto a G-25 Sephadex column, in 20 mM potassium phosphate buffer (pH 6). The protein was collected and subsequently loaded onto a CM-52 column, in 20 mM potassium phosphate (KP) buffer. The column was then rinsed with 20 mM KP buffer, and then the protein was eluted with 100 mM KP (pH 6). The protein was centrifuged to increase the concentration as needed.

Spectroscopic Analyses. All UV−vis spectra were collected using a Hewlett-Packard 8453 UV−vis spectrophotometer. The DHP and mutant purity was calculated as the A_{406}/A_{280} ratio. A 0.4 cm path length was used for kinetic assays, while a 1.0 cm path length was used for standard UV−vis spectra.

Resonance Raman. Resonance Raman spectra were obtained by excitation of the Soret band at 409 nm using a frequency-doubled Ti:sapphire laser. The 10 W beam of 532 nm light from a Coherent Verdi laser was used to generate 818 nm light in a Coherent Mira 900 Ti:sapphire laser. The resulting beam was frequency doubled using a Coherent 5-050 doubler to generate 409 nm light as the excitation source for the resonance Raman experiments. The laser output was calibrated using Rayleigh scattering, toluene, and cyclohexane standards. The excitation source was collimated and cylindrically focused to a vertical line of ∼0.5 mm and ∼60 mW at the sample. Raman scattered light passed through a Spex 1877 Triplemate monochromator and was detected by a liquid N_2-cooled CCD camera (ISA Spex, model CCD-3000). Samples were placed in 5 mm NMR tubes and spun with an air piston spinning sample holder (Princeton Photonics, model Raman 101). Spectra were measured at room temperature for three acquisitions with exposure times of 300 s, alternating between samples. Each sample scan was repeated three times and averaged to improve the signal-to-noise ratio.

Kinetic Assays. For all kinetic assays, the concentration of DHP mutants was 2.5 μM. The concentration of 4-BP was 125 μM for the 1:1 comparisons and 250 μM for the 2:1 comparisons. The concentration for TCP was 125 μM. These contents were added to the cuvette, and the cuvette was filled to 1 mL with 100 mM KP buffer; 200 μL of 1 mM H_2O_2 was added at the start of each kinetic assay. Previous studies have shown that DHP activity requires the addition of substrate, TCP, prior to the cosubstrate, H_2O_2.[19]

Molecular Dynamics Simulations. Molecular dynamics (MD) simulations were conducted using the molecular dynamics program NAMD.[33,34] The initial coordinates were obtained from the Protein Data Bank (entry 2QFK).[16] Mutations were created using the Mutate Residue module of the visual molecular dynamics program VMD.[35] NAMD simulations were conducted on monomer DHP mutants in the L100 position with periodic boundary conditions in a water box. The dimensions of the boxes are roughly 60 Å × 60 Å × 64 Å, and ∼9250 water molecules were used to solvate the DHP mutants. The cutoffs used in the simulation are 12 Å, with a standard switching function. The time used was 2 fs because bonds to H atoms were restrained using the SHAKE algorithm.

X-ray Crystallography. Recombinant non-His_6-tagged L100F protein, which is necessary for crystallization, was expressed in *E. coli*, purified, and characterized as previously described.[16] Crystals of non-His_6-tagged L100F were grown using the hanging drop vapor diffusion method at 298 K by mixing 3 μL of protein solution [8 mg/mL in 10 mM sodium cacodylate buffer (pH 6.5)] and 3 μL of reservoir solution [unbuffered 0.2 M ammonium sulfate and 32% PEG 4000 (w/v)] in a Hampton Research VDX plate as described previously.[16,27] Crystals of L100F complexed with 4-BP were obtained similarly, but the protein solution was incubated on ice for 30 min with the 10 mM 4-bromophenol prior to setting up the hanging drops. The crystals were cryoprotected in a solution containing 0.2 M ammonium sulfate, 32% PEG 4000 (w/v), and 20% glycerol (v/v). Data were collected at 100 K on the SER-CAT 22-ID beamline at the APS synchrotron facility using a wavelength of 1 Å. The collected diffraction data sets were processed using the HKL2000 program suite.[36] The new crystals belong to the same space group, $P2_12_12_1$, as the ferric water-ligated (metaquo) form (PDB entry 2QFK), and the structures were determined using the Phaser molecular replacement program[37] with PDB entry 2QFK as the search model. Manual model building was conducted using Coot model building software.[38] Waters were placed with the Coot routine Find Waters. The final models were obtained by iterative cycles of model building in Coot and structure refinement using Refmac5[39] in the CCP4 suite of programs (Collaborative Computational Project, 1994). Figures were prepared with Chimera. Refinement statistics are listed in Table 1.

RESULTS

Kinetic assays were completed to compare the rate of formation of 2,6-DCQ by each mutant to that of WT DHP by measuring the change in absorbance at 273 nm (Figure 1). Product, 2,6-DCQ, formation leads to an increase in absorbance at 273 nm, but the hydroxylation of 2,6-DCQ accounts for the decrease in absorbance at 273 nm at longer times in the data shown in Figure 1. Hydroxylation of 2,6-DCQ to produce 3-hydroxy-2,6-DCQ occurs spontaneously as a secondary reaction in solution,[40] but the rate of this process is nearly 1 order of magnitude lower than the rate of 2,6-DCQ formation and has generally been ignored in the kinetic analyses of DHP.[26,41,42] While we can separate the time scale of the slower hydroxylation process from that of the more rapid oxidation of 2,4,6-TCP and thereby determine the Michaelis−Menten parameters, the overall yield of 2,6-DCQ appears to differ for the different mutants. Examination of Figure 1 reveals that an increase in the level of substrate oxidation also results in an increase in the rate of the secondary hydroxylation reaction as we have described previously.[40] This aspect is not simply identified by Michaelis−Menten kinetics. Therefore, in this work, we have separately considered the factors governing the oxidation using the short-time approximation and studied the effects of mutations on the longer time scale hydroxylation process.

Upon addition of the 4-BP inhibitor, L100V and L100Q show a significant decrease in the rate of substrate turnover as shown in Figure 1. The kinetic results from the substrate-only experiment of L100T suggest that L100T produces a significant amount of 3-hydroxy-2,6-DCQ as indicated by the shape of the

Table 1. Data Collection and Refinement Statistics

	L100F	L100F−4-BP
PDB entry	4HSW	4HSX
space group	$P2_12_12_1$	$P2_12_12_1$
unit cell parameters		
a (Å)	57.59	58.24
b (Å)	66.73	67.44
c (Å)	69.22	69.34
Data Collection[a]		
temperature (K)	100	100
wavelength (Å)	1.000	0.9184
resolution (Å)	48.042−1.22 (1.24−1.22)	48.35−1.12 (1.14−1.12)
no. of unique reflections	79901	105290
completeness (%)	99.9 (100)	99.9 (98.7)
R_{merge} (%)[b]	6.3 (37.2)	7.9 (24.2)
I/a	41.30 (4.35)	26.19 (3.24)
redundancy	7.2 (6.1)	3.7 (3.1)
Refinement		
R_{work}/R_{free} (%)[c]	13.32/16.39	12.56/15.03
average *B* factor (Å^2)		
all atoms	14.41	10.89
protein	12.91	9.24
water	23.66	20.56
no. of atoms		
protein	2419	2436
water	373	416
rmsd from ideal		
bond lengths (Å)	0.026	0.03
bond angles (deg)	3.55	3.52
Ramachandran plot (%)		
most favored	98.7	98.7
allowed	1.3	1.3

[a]Values in parentheses are for the highest-resolution shell. [b]$R_{merge} = \sum(|I - \bar{I}|)/\sum I \times 100$. [c]$R_{work} = \sum|F_o - F_c|/\sum F_o \times 100$, where F_o is the observed structure factor amplitude and F_c is the calculated structure factor amplitude.

kinetic trace. As the turnover rate becomes faster than WT DHP, the concentration of the radical intermediate builds up sufficiently rapidly that the secondary reaction begins to compete with the primary turnover of 2,4,6-TCP. As the inhibitor concentration increases, the L100T spectra begin to resemble those of WT DHP. The inhibition assays suggest that L100T and L100F are the least inhibited by 4-BP of any of the DHP mutants studied (or the wild type). On the basis of the initial slopes of the uninhibited kinetic trace, the mutants may be ranked in terms of substrate turnover frequency: L100F < L100V < L100Q < WT < L100T. Kinetic experiments were also conducted to obtain Michealis−Menten parameters and assess the efficiency of each mutant to catalytically convert both 2,4,6-TCP and 4-BP. These data are summarized in Tables 2 and 3. Plots of the Michaelis−Menten assays are available in the Supporting Information.

Table 2 suggests that the catalytic rate of L100Q is similar in magnitude to that of WT DHP. Using the k_{cat}/K_m ratio, the mutants can be ranked in efficiency as follows: L100F < L100V < WT < L100T < L100Q. These data suggest that the two mutants with polar mutations at the L100 site have a higher catalytic efficiency for the turnover of 2,4,6-TCP than WT DHP, while the two mutants with nonpolar mutations have a lower catalytic efficiency.

Table 3 summarizes the ability of each mutant to turn over 4-BP in comparison to that of WT DHP. Although 4-BP is considered an inhibitor for 2,4,6-TCP catalysis, it does have a measurable rate of turnover. The k_{cat}/K_m values for oxidation of 4-BP by each mutant are approximately an order of magnitude smaller than the values for the 2,4,6-TCP conversions. At the highest 4-BP concentrations, L100F turns over 4-BP twice as fast as WT DHP, and L100T approaches the catalytic rate maximum of WT DHP for this conversion (see Figure S2 of the Supporting Information). The ranking of catalytic efficiency according to the k_{cat}/K_m values is as follows: L100T < L100Q < L100V < L100F < WT. These data suggest that the L100 mutants with nonpolar mutations turn over 4-BP with a higher catalytic efficiency than the mutants with polar mutations, which is the opposite of the order of the reactivity toward the substrate.

Resonance Raman studies of DHP have provided information based on the observation of the core size marker modes, and in particular the ν_3 mode.[8,43,44] On the basis of the correlation of the resonance Raman data with X-ray crystal structures, it has been suggested that axial ligation of H_2O and perhaps other ligands to ferric heme iron is linked to the conformation of the distal histidine.[8] The observed correlation is that H55 is stabilized in an internal conformation when H_2O is bound to the heme Fe (six-coordinate high-spin type) and is observed in an external conformation when the heme iron is a five-coordinate high-spin type (with no water bound to the heme Fe). This view of the conformation of H55 is commensurate with the requirement that the closed (internal) conformation can form hydrogen bonds to axial ligands bound to the heme iron, which is essential for catalysis of Fe−H_2O_2 to form the active Compound I.[32] Additionally, because the bound inhibitor molecule displaces the water coordinated to the heme iron in the distal cavity, the coordination of H_2O_2 is prevented and peroxidase activity of the enzyme is inhibited.[8] Therefore, H55 in the internal position stabilizes the six-coordinate high-spin (6cHS) state, and H55 in the external position gives rise to the five-coordinate high-spin (5cHS) state.[8,27,32] The ν_3 core size marker mode, which ranges from 1470 to 1510 cm^{-1} in WT DHP, has been suggested for use in analysis because of its isolation in the WT DHP RR spectrum.[45] The Raman results for addition of 125 μM 4-BP to each 2.5 μM mutant are shown in Figure 2. An increased population of 6cHS heme indicates that a water molecule is bound to the heme iron. The ligand is assigned as H_2O both because of the shape of the absorption and Raman spectra and because no other axial ligands are present in the experiment. When H_2O is bound, H55 is observed in the closed conformation. This observation suggests that the monohalogenated inhibitor is not present in the heme pocket and the protein can freely oxidize trihalogenated phenols. An increased population of 5cHS iron indicates that an inhibitor has entered the heme pocket, displacing the previously bound water molecule and pushing H55 to the open position. Upon addition of 4-BP, 6cHS peaks are pronounced in the ν_2 region of the L100F spectrum and both ν_3 and ν_2 regions of the L100T spectrum. L100Q shows prevalent 5cHS peaks in ν_3 and ν_2. The L100V sample was prone to aggregation under excitation conditions of the Raman experiment, and no data were obtained.

Diffraction quality protein crystals were obtained only for the L100F mutant. The structure of L100F was obtained to 1.22 Å resolution and is homologous to that of WT DHP with the exception of the single point mutation. Like WT DHP, the

dx.doi.org/10.1021/bi301509r | *Biochemistry* 2013, 52, 2218−2227

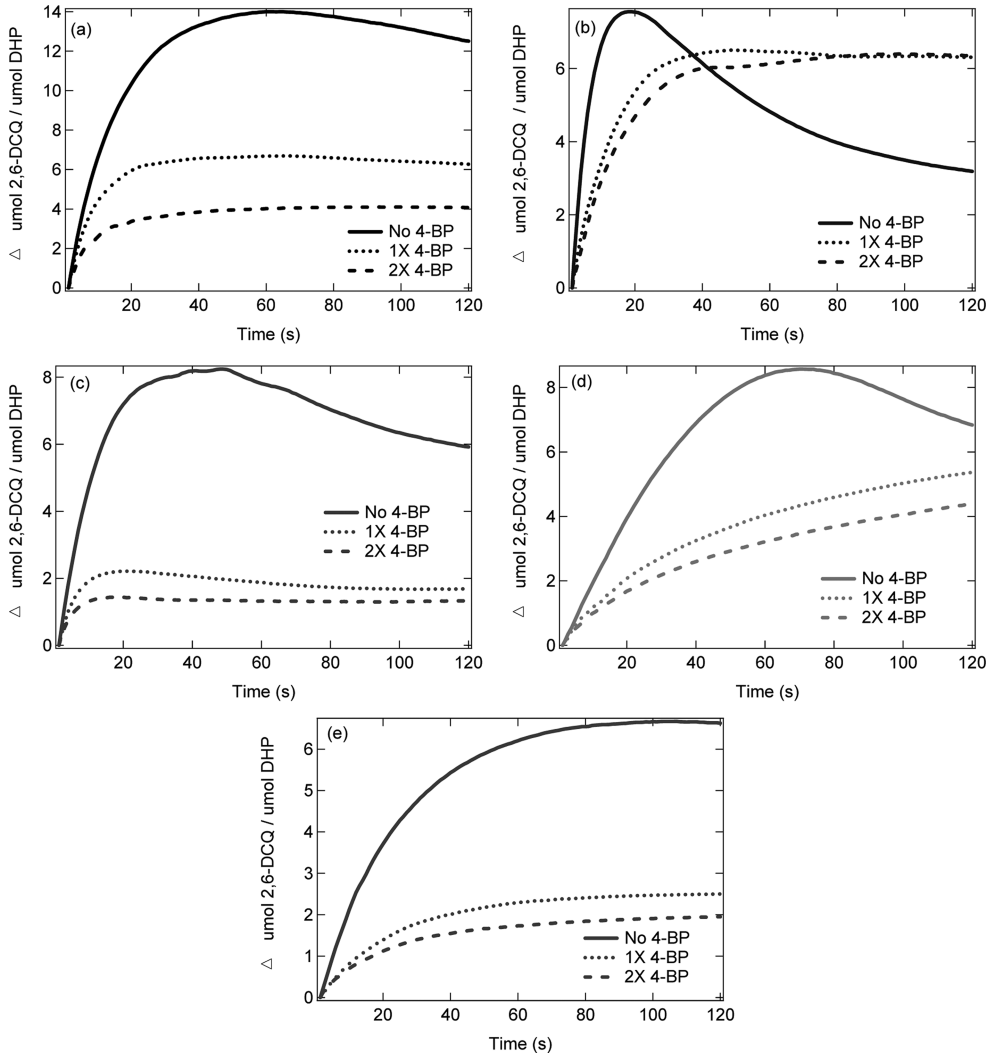

Figure 1. Inhibition assays show the absorbance at 273 nm with the addition of TCP only, TCP and 4-BP (1:1 ratio), or TCP and 4-BP (1:2 ratio) to WT DHP (a), L100T (b), L100Q (c), L100F (d), and L100V (e).

Table 2. Michaelis–Menten Parameters for 2,4,6-TCP as a Substrate

	K_m (μM)	k_{cat} (s^{-1})	k_{cat}/K_m ($\times 10^{-3}$ μM^{-1} s^{-1})
WT	1900 ± 382	10.34 ± 1.44	5.45 ± 1.34
L100F	2220 ± 572	7.56 ± 1.41	3.41 ± 1.09
L100T	275 ± 67.7	3.09 ± 0.26	11.2 ± 2.92
L100Q	654 ± 77.8	11.58 ± 0.67	17.7 ± 2.34
L100V	870 ± 52.1	4.57 ± 0.15	5.25 ± 0.357

Table 3. Michaelis–Menten Parameters for 4-BP as a Substrate

	K_m (μM)	k_{cat} (s^{-1})	k_{cat}/K_m ($\times 10^{-4}$ μM^{-1} s^{-1})
WT	152 ± 16.8	0.232 ± 0.007	15.3 ± 1.75
L100F	471 ± 79.5	0.425 ± 0.028	9.03 ± 1.64
L100T	1090 ± 457	0.383 ± 0.094	3.50 ± 1.69
L100Q	246 ± 54.9	0.175 ± 0.012	7.09 ± 1.65
L100V	274 ± 86.7	0.200 ± 0.020	7.28 ± 2.42

distal H55 is observed in the closed position as shown by the electron density in the axial sixth position of the heme Fe. As for the WT structure, the unusual axial electron density was fit with a water molecule coordinated to the Fe, stabilized by hydrogen bonding to the distal H55. The density has been attributed to photoreduction of the heme Fe[16,46] and any resulting photoreduced products. Nevertheless, the closed conformation of the distal H55 in the absence of 4-BP is in agreement with the RR spectra presented here and the previous mechanism of action for DHP.[8,21]

The crystal structure of L100F in the presence of 4-BP was determined to 1.12 Å resolution. Figure 3 shows that the omit map, contoured at 3σ, can be fit with a heme-coordinated water molecule, 4-BP, and two conformations (open and closed) of the distal H55. The occupancy of the 4-BP molecule is 0.375 averaged over the two active sites, and the occupancies of the open and closed conformations of the distal H55 are 0.60 and 0.40, respectively, averaged over the two active sites. Thus, in agreement with the RR spectra presented in Figure 2, addition of 4-BP to DHP results in both 5cHS and 6cHS populations of L100F DHP. The inhibitor, 4-BP, is accommodated well in the distal pocket despite the increase in steric bulk due to the L100F mutation as shown in Figures S5–S7 of the Supporting Information. The 4-BP molecule is actually situated slightly deeper in the distal pocket than in the wild-type structure with bound 4-BP (PDB entry 3LB2). For example, the distance from the OH group of 4-BP and the position 7 propionate O atom is

dx.doi.org/10.1021/bi301509r | *Biochemistry* 2013, 52, 2218–2227

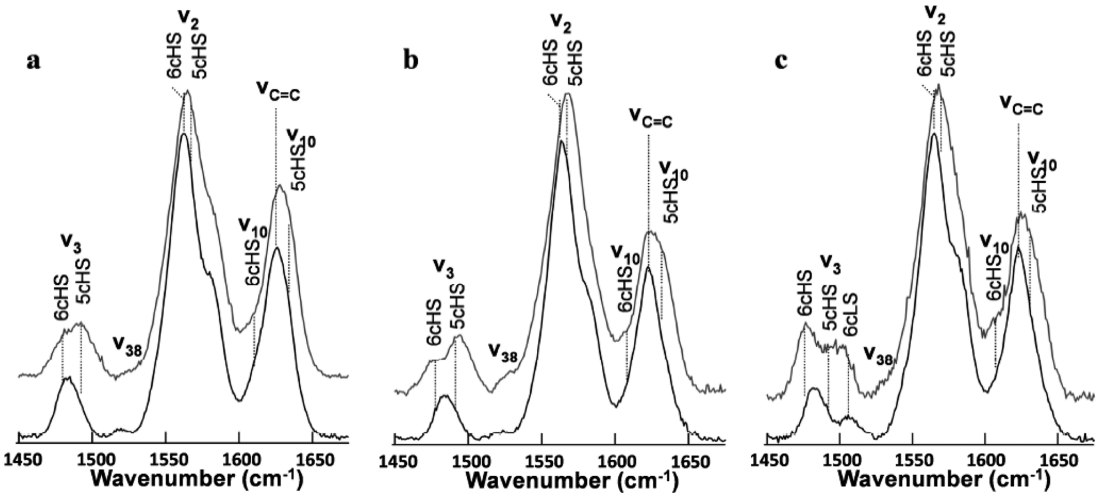

Figure 2. Resonance Raman spectra for L100F (a), L100Q (b), and L100T (c). The bottom spectra show each mutant with neither substrate nor inhibitor. The top spectra show each mutant in the presence of 2 mM 4-BP.

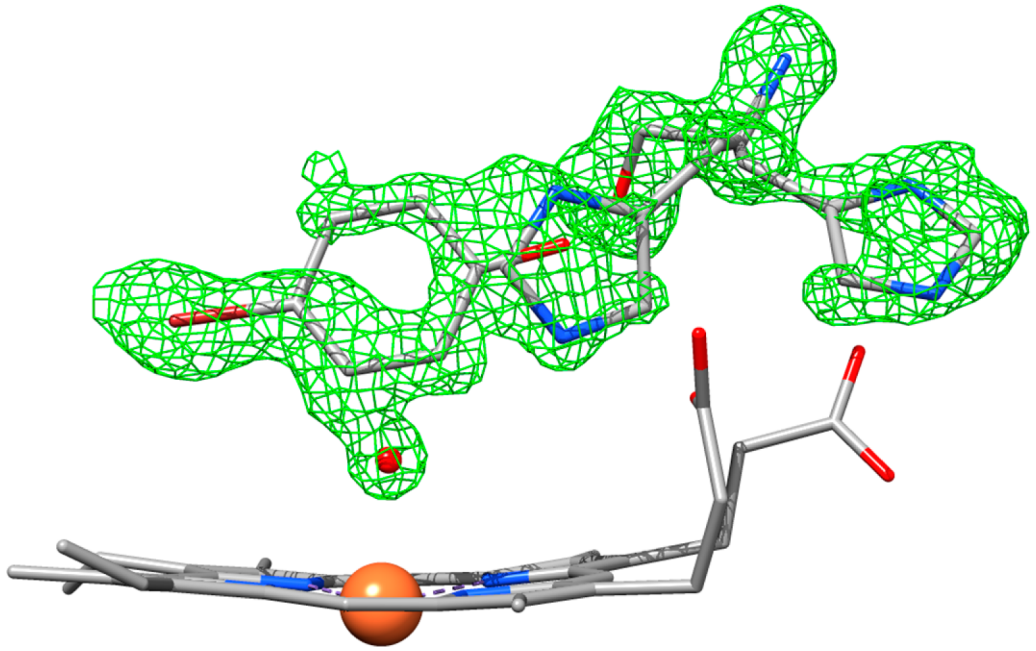

Figure 3. Electron density, contoured at 3σ, can be fit with a heme-coordinated water molecule, a 4-BP molecule, and two conformations of the distal H55. This model is in agreement with previously published literature regarding the mechanism of DHP.

2.8 Å in the wild type (PDB entry 3LB2) and 3.1 Å in the L100F mutant (PDB entry 4HSX). F100 is pushed up 0.1 Å farther from the heme Fe by the para-Br atom of 4-BP. The geometry of the inhibitor in the distal pocket is shown in Figure 4 with a calculation using the utility SURFNET to show the protein cavity in the distal pocket of DHP (PDB entry 3LB2). In both structures (4HSW and 4HSX), F100 makes a strong T-shaped interaction with the neighboring F101.

Molecular dynamics simulations were conducted to predict the spatial interactions between each L100 mutant and the inhibitor molecule. The distances between the heme Fe and either Br or OH of the 4-BP inhibitor are summarized in Table 4 or 5, respectively. In addition, the time course analyses for each mutant are provided in Figure S4 of the Supporting Information. The Fe−OH and Fe−Br distances in L100Q remain relatively stable, with average values of 7.14 and 4.42 Å, respectively, and the lowest standard deviations of the mutants. The standard deviations for L100F are slightly greater than that of L100Q, but the average distances are comparable. The L100T simulations differed significantly from those for the other mutants. The maximal Fe−Br distance reaches 11.4 Å, and the minimal Fe−OH distance reaches 2.60 Å. These data may suggest the relative instability of 4-BP in the distal cavity of the L100T mutant.

DISCUSSION

Our initial hypothesis was based on the idea that steric control may play a prominent role in binding of the 4-BP inhibitor in the heme cavity of DHP.[19] Experience with previous mutants, the Xe-binding site,[19] and the effect of halogen size on the bound inhibitors[8] led to the idea that increasing the size of the hydrophobic cavity for the para-bromine atom may destabilize the binding of 4-BP. We now suggest that changes in the polarity of the amino acid residues also have a profound effect

dx.doi.org/10.1021/bi301509r | *Biochemistry* 2013, 52, 2218−2227

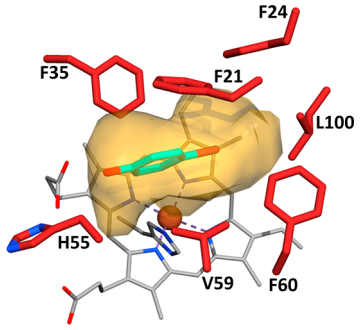

Figure 4. X-ray crystal structure of DHP with the inhibitor, 4-BP (cyan), showing the size and location of the hydrophobic distal heme pocket (transparent orange). The bromine of 4-BP is surrounded by several hydrophobic residues (red), including F21, F24, F35, V59, F60, and L100. This figure was prepared using the Surfnet feature of Chimera that identifies molecular cavities and indentations in proteins.[47] PDB entry 3LB2 was used to make this figure.

Table 4. Statistical Analysis of the Distances between the Heme Iron and the Br of 4-BP in the LI00 Mutants

	L100F	L100Q	L100T	WT
Maximum	7.423	6.871	11.361	7.171
Minimum	2.583	2.533	2.572	3.203
Average	4.311	4.42	5.08	4.498
Standard Deviation	0.568	0.429	1.446	0.391

Table 5. Statistical Analysis of the Distances between the Heme Iron and the OH of 4-BP in the LI00 Mutants

	L100F	L100Q	L100T	WT
Maximum	9.383	9.052	9.207	9.718
Minimum	4.599	4.54	2.598	3.619
Average	7	7.143	6.59	6.868
Standard Deviation	0.62	0.368	0.795	0.418

on the binding of the inhibitor and rate of enzymatic reaction. This may be due to the distal pocket of DHP being more hydrophobic than that of typical globins because the heme is more deeply buried in the cleft of the globin.[32]

Inhibition kinetic experiments with the L100 mutants suggest that L100T can produce more 2,6-DCQ product than the wild type in the presence of 4-BP. This suggests the destabilization of inhibitor binding by introducing a slightly polar residue into the hydrophobic heme cavity, which may also stabilize substrate binding. Resonance Raman experiments confirm this with the presence of 6cHS peaks (Figure 2), which correspond to H_2O being bound to the heme Fe. This destabilization is further corroborated by MD simulations, which show large fluctuations in the distances between the heme Fe and the 4-BP inhibitor. These results indicate that 4-BP is not stable in the distal pocket of L100T. An increase in the polarity of the distal pocket leads to an apparent increase in the catalytic efficiency (k_{cat}/K_m) of the native function of the enzyme, as shown by Michaelis–Menten parameters obtained from our analysis (Table 2). The greatest effect of the increased polarity appears to be an increase in the on rate for substrate binding. Thus, solvent polarity in the L100T mutant can play a dual role in the increased catalytic efficiency and the simultaneous reduction of the inhibitory effect of 4-BP. The kinetic data for 2,4,6-TCP oxidation are complicated by the increased level of production of 3-hydroxy-2,6-DCQ (Figure 1), which is a known phenomenon when the rate of oxidation is increased substantially.[40] The kinetics of the L100T mutant indicate that hydroxylation is quite rapid in the absence of inhibitor but is reduced dramatically in the presence of 4-BP. The role of the inhibitor appears to compete with hydroxylation, resulting in an increase in the yield of product, despite the fact that the initial rate of product formation is lower in the presence of the inhibitor. This is a case where the method of initial rates, used universally in Michaelis–Menten kinetic analysis, does not represent the product yield. Because these effects are not observed in the isosteric L100V mutant, it appears that the increased polarity of the amino acid T plays a role in the enhanced activity and lack of inhibition.

Clearly, steric effects alone are not sufficient to destabilize inhibitor binding because decreasing the size of the L100 residue, as observed in the L100V mutant, increases the level of inhibition of 2,6-DCQ formation. Because L100V and L100T are isosteric, they provide the clearest comparison of the steric effect separated from the polarity effect. L100V does not greatly affect the catalytic efficiency of DHP but does increase the effect of 4-BP inhibition slightly. On the other hand, L100T both increases the catalytic efficiency for 2,4,6-TCP and decreases the level of inhibition.

The Michaelis–Menten experiments suggest that L100Q also has a higher catalytic efficiency for 2,4,6-TCP turnover than WT DHP. However, unlike L100T, the L100Q mutant shows a prevalent 5cHS Raman peak and also loses ability to turn over 2,4,6-TCP with the addition of 4-BP. In the case of L100T, the introduction of a polar residue into the distal heme cavity of DHP may be associated with a lower affinity for 4-BP as an inhibitor. Of course, one cannot completely separate the steric effect of these two mutants. The L100T mutant actually enlarges the protein cavity of the Xe binding site. On the other hand, the L100Q mutant significantly decreases the size of the cavity. The inhibitor appears to bind well despite the smaller cavity in the L100Q mutant. This observation fits with other data showing that a reduction in the size of the distal cavity does not destabilize inhibitor binding. In the case of L100Q, the steric effect may be too large to differentiate between the possible polarity change introduced into the distal cavity.

The steric hindrance provided by the introduction of the bulky phenyl ring of L100F is of interest because this bulkiness could potentially limit the access of 4-BP to the distal cavity. A simple steric argument would suggest that this effect would be the largest steric effect of any mutation studied here. Resonance Raman experiments suggest that L100F has a lower affinity for 4-BP as an inhibitor because there is an increased population of the 6cHS form as compared to that of WT DHP. When 4-BP is added to WT DHP, the heme is converted to nearly 100% 5cHS, while for L100F, only a small amount of the 6cHS species is converted to 5cHS, suggesting a lower affinity for internal binding. In addition, the inhibition assays showed only a small decrease in enzymatic activity with the addition of inhibitor. Although L100F may sterically hinder the presence of 4-BP in the distal cavity, the amount of 2,4,6-TCP turned over by L100F does not surpass the amount with WT DHP. Inhibition appears to be maintained. The conclusion must be that despite the larger steric bulk of the phenyl ring, the inhibitor 4-BP can bind in the distal pocket. The two X-ray crystal structures of the L100F mutant, with and without bound 4-BP, support this idea. The F100 residue is rotated so that it makes a T shape with respect to F101. This structure maintains

dx.doi.org/10.1021/bi301509r | *Biochemistry* 2013, 52, 2218–2227

a cavity in the protein that is capable of accommodating the para-Br atom of 4-BP with minimal structural rearrangement.

The idea that 4-BP can bind in the distal pocket of the L100F mutant is strongly corroborated by the X-ray crystal structure of L100F with bound 4-BP. The electron density in the distal cavity for the L100F−4-BP species is explained as a mixture of two states. Given that the RR spectrum of L100F in the presence of 4-BP produces populations of both 5cHS and 6cHS heme corresponding to the open (4-BP bound) and closed (4-BP not bound) conformations of the distal H55, the electron density could have been predicted to consist of contributions from these two forms of DHP. Fitting the density with both conformations of the distal H55, a 4-BP molecule, and a water molecule coordinated to the heme Fe is in complete agreement with the overall mechanism of action for DHP that has been very well characterized. Internal binding of 4-BP displaces the water molecule and pushes the distal H55 to the open conformation. Because the L100F mutation lowers the internal binding affinity, the occupancy of 4-BP in the distal pocket is approximately 37.5%. Both species, 5cHS with 4-BP and 6cHS without 4-BP, are observed in the crystal with occupancies of 0.375 and 0.625, respectively. On the other hand, for WT DHP, binding of 4-BP results is nearly 100% 5cHS seen in RR and 100% occupancy of 4-BP in the distal pocket.

An interesting observation is that binding of 4-BP in the distal cavity of DHP seems to produce the best diffraction quality crystals. The structures of WT DHP with 4-BP (1.06 Å resolution) and L100F with 4-BP (1.12 Å resolution) are the highest-resolution structures of DHP obtained to date. While we cannot say with certainty that internal binding of 4-BP stabilizes the enzyme, such a suggestion would explain these two significant instances, in which 4-BP binding yields protein crystals that are higher in quality than the same crystal form without inhibitor. Because 4-BP is one of the natural phenols encountered by DHP, it seems likely that DHP has evolved to bind 4-BP with high specificity.[8] This observation is important because it demonstrates the high specificity of inhibitor binding that we have attempted to overcome with the series of L100 mutants. The hydrophobic cavity appears to be able to conform to the inhibitor, even in certain mutants. Thus, the plasticity of the overall globin structure prevents steric effects from being the decisive factor that governs inhibitor binding. Instead, the introduction of a hydroxyl group in L100T appears to have had the crucial effect that destabilized inhibitor binding.

CONCLUSION

The polarity effect of amino acid mutations at the L100 position has been shown to be important, in addition to the steric effect, in affecting the stability of inhibitor binding. Increased polarity introduced by the L100T mutation decreases the binding affinity of the inhibitor, but it also appears to increase the on rate for substrate binding. The opposition of inhibitor and substrate binding is a central feature of the two-site competitive inhibition of DHP.[8] The mutations at the L100 position provide a deeper understanding of the role played by the distal pocket in the mechanism because they indicate the cavity in the protein is designed to be hydrophobic to stabilize the bromine atom of the inhibitor. Apart from the rate of product formation, the L100T mutant shows an increased total yield of product in the presence of 4-BP, which must result from a decrease in the effective rate of the secondary hydroxylation reaction. In contrast to the polar mutations, the nonpolar L100 mutants possess a higher affinity for 4-BP inhibition. This is coupled with a decrease in the catalytic efficiency due mainly to a lower catalytic rate. In peroxidase reactions, this implies a poorer activation of bound H_2O_2.[2,26] Of course, increased polarity may adversely affect the globin function, which may explain why the evolution of the distal pocket has resulted in an extremely hydrophobic environment in DHP. A dual-function protein is inherently a compromise between different requirements for the various functions. The hydrophobicity of the distal pocket affects the binding of CO and O_2 and the autoxidation rate of Fe^{2+}, all of which are key factors in determining the efficacy of the O_2 transport function. These issues will be investigated further in comparative studies of the globin function, to understand the evolution of DHP and the context of its multiple functions.

ASSOCIATED CONTENT

Supporting Information

Primers, Michaelis−Menten kinetic data, UV−vis spectral recordings of assays, comparisons of critical amino acids in X-ray structures, dimensions of the inhibitor binding cavity, and distances relevant to MD simulations. This material is available free of charge via the Internet at http://pubs.acs.org.

Accession Codes

PDB entries 4HSW and 4HSX.

AUTHOR INFORMATION

Corresponding Author

*Department of Chemistry, North Carolina State University, Raleigh, NC 27695. E-mail: stefan_franzen@ncsu.edu. Phone: (919) 515-8915.

Funding

This work was supported Army Research Office Grant 56871-LS.

Notes

The authors declare no competing financial interest.

ABBREVIATIONS

DHP, dehaloperoxidase-hemoglobin; HRP, horseradish peroxidase; MD, molecular dynamics; 4-BP, 4-bromophenol; PDB, Protein Data Bank; 2,4,6-TCP, 2,4,6-trichlorophenol; SWMb, sperm whale myoglobin; IPTG, isopropyl β-D-1-thiogalactopyranoside; WT, wild-type.

REFERENCES

(1) Chen, Y. P., Woodin, S. A., Lincoln, D. E., and Lovell, C. R. (1996) An unusual dehalogenating peroxidase from the marine terebellid polychaete *Amphitrite ornata*. *J. Biol. Chem. 271*, 4609−4612.

(2) Dunford, B. H. (1999) *Heme Peroxidases*, John Wiley and Sons, New York.

(3) Weber, R. E., Mangum, C., Steinman, H., Bonaventura, C., Sullivan, B., and Bonaventura, J. (1977) Hemoglobins of two terebellid polychaetes: *Enoplobranchus sanuineus* and *Amphitrite ornata*. *Comp. Biochem. Physiol., Part B: Biochem. Mol. Biol.*, 179−187.

(4) Argese, E., Bettiol, C., Giurin, G., and Miana, P. (1999) Quantitative structure-activity relationships for the toxicity of chlorophenols to mammalian submitochondrial particles. *Chemosphere 38*, 2281−2292.

(5) Godoy, F., Zenteno, P., Cerda, F., Gonzalez, B., and Martinez, M. (1999) Tolerance to trichlorophenols in microorganisms from a polluted and a pristine site of a river. *Chemosphere 38*, 655−662.

(6) Osborne, R. L., Raner, G. M., Hager, L. P., and Dawson, J. H. (2006) *C. fumago* Chloroperoxidase is also a Dehaloperoxidase: Oxidative Dehalogenation of Halophenols. *J. Am. Chem. Soc. 128*, 1036−1037.

(7) Lincoln, D. E., Fielman, K. T., Marinelli, R. L., and Woodin, S. A. (2005) Bromophenol accumulation and sediment contamination by the marine annelids *Notomastus lobatus* and *Thelepus crispus*. *Biochem. Syst. Ecol. 33*, 559−570.
(8) Thompson, M. K., Davis, M. F., de Serrano, V., Nicoletti, F. P., Howes, B. D., Smulevich, G., and Franzen, S. (2010) Internal Binding of Halogenated Phenols in Dehaloperoxidase-Hemoglobin Inhibits Peroxidase Function. *Biophys. J. 99*, 1586−1595.
(9) Thompson, M. K., Franzen, S., Davis, M. F., Oliver, R. C., and Krueger, J. K. (2011) Dehaloperoxidase-Hemoglobin from *Amphitrite ornata* Is Primarily a Monomer in Solution. *J. Phys. Chem. B 115*, 4266−4272.
(10) Han, K., Woodin, S. A., Lincoln, D. E., Fielman, K. T., and Ely, B. (2001) *Amphitrite ornata*, a marine worm, contains two dehaloperoxidase genes. *Mar. Biotechnol. 3*, 287−292.
(11) de Serrano, V., D'Antonio, J., Franzen, S., and Ghiladi, R. A. (2010) Structure of dehaloperoxidase B at 1.58 angstrom resolution and structural characterization of the AB dimer from *Amphitrite ornata*. *Acta Crystallogr. D66*, 529−538.
(12) D'Antonio, J., D'Antonio, E. L., Thompson, M. K., Bowden, E. F., Franzen, S., Smirnova, T., and Ghiladi, R. A. (2010) Spectroscopic and Mechanistic Investigations of Dehaloperoxidase B from *Amphitrite ornata*. *Biochemistry 49*, 6600−6616.
(13) Lebioda, L., LaCount, M. W., Zhang, E., Chen, Y. P., Han, K., Whitton, M. M., Lincoln, D. E., and Woodin, S. A. (1999) An enzymatic globin from a marine worm. *Nature 401*, 445.
(14) de Serrano, V., D'Antonio, J., Franzen, S., and Ghiladi, R. A. (2010) Crystal structure of dehaloperoxidase B at 1.58 Å and characterization of the A/B dimer from *Amphitrite ornata*. *Acta Crystallogr. D66*, 529−538.
(15) LaCount, M. W., Zhang, E. L., Chen, Y. P., Han, K. P., Whitton, M. M., Lincoln, D. E., Woodin, S. A., and Lebioda, L. (2000) The crystal structure and amino acid sequence of dehaloperoxidase from *Amphitrite ornata* indicate common ancestry with globins. *J. Biol. Chem. 275*, 18712−18716.
(16) de Serrano, V., Chen, Z. X., Davis, M. F., and Franzen, S. (2007) X-ray crystal structural analysis of the binding site in the ferric and oxyferrous forms of the recombinant heme dehaloperoxidase cloned from *Amphitrite ornata*. *Acta Crystallogr. D63*, 1094−1101.
(17) Davis, M. F., Bobay, B. G., and Franzen, S. (2010) Determination of Separate Inhibitor and Substrate Binding Sites in the Dehaloperoxidase-Hemoglobin from *Amphitrite ornata*. *Biochemistry 49*, 1199−1206.
(18) Nienhaus, K., Nickel, E., Davis, M. F., Franzen, S., and Nienhaus, G. U. (2008) Determinants of Substrate Internalization in the Distal Pocket of Dehaloperoxidase Hemoglobin of *Amphitrite ornata*. *Biochemistry 47*, 12985−12994.
(19) de Serrano, V., and Franzen, S. (2012) Structural Evidence for Stabilization of Inhibitor Binding by a Protein Cavity in the Dehaloperoxidase-Hemoglobin from *Amphitrite ornata*. *Biopolymers 98*, 27−35.
(20) Franzen, S., Thompson, M. K., and Ghiladi, R. A. (2012) The Dehaloperoxidase Paradox. *Biochim. Biophys. Acta 1824*, 578−588.
(21) Thompson, M. K., Franzen, S., Ghiladi, R. A., Reeder, B. J., and Svistunenko, D. A. (2010) Compound ES of Dehaloperoxidase Decays via Two Alternative Pathways Depending on the Conformation of the Distal Histidine. *J. Am. Chem. Soc. 132*, 17501−17510.
(22) Davis, M. F., Gracz, H., Vendeix, F. A., de Serrano, V., Somasundaram, A., Decatur, S. M., and Franzen, S. (2009) Different Modes of Binding of Mono-, Di-, and Trihalogenated Phenols to the Hemoglobin Dehaloperoxidase from *Amphitrite ornata*. *Biochemistry 48*, 2164−2172.
(23) Ferrari, R. P., Laurenti, E., and Trotta, F. (1999) Oxidative 4-dechlorination of 2,4,6-trichlorophenol catalyzed by horseradish peroxidase. *JBIC, J. Biol. Inorg. Chem. 4*, 232−237.
(24) Laurenti, E., Ghibaudi, E., Ardissone, S., and Ferrari, R. P. (2003) Oxidation of 2,4-dichlorophenol catalyzed by horseradish peroxidase: Characterization of the reaction mechanism by UV-visible spectroscopy and mass spectrometry. *J. Inorg. Biochem. 95*, 171−176.
(25) de Serrano, V. S., Zhao, J., and Franzen, S. (2013) Structural and kinetic study of an internal substrate binding site of dehaloperoxidase-hemoglobin A from *Amphitrite ornata*. *Biochemistry 52*, DOI: 10.1021/bi301307f.
(26) Ma, H., Thompson, M. K., Gaff, J., and Franzen, S. (2010) Kinetic Analysis of a Naturally Occurring Bioremediation Enzyme: Dehaloperoxidase-Hemoglobin from *Amphitrite ornata*. *J. Phys. Chem. B 114*, 13823−13829.
(27) Chen, Z., de Serrano, V., Betts, L., and Franzen, S. (2009) Distal histidine conformation flexibility in dehaloperoxidase from *Amphitrite ornata*. *Acta Crystallogr. D65*, 34−40.
(28) Sage, J. T., Li, P., and Champion, P. M. (1991) Spectroscopic studies at low pH: Heme ligation kinetics. *Biochemistry 30*, 1237−1247.
(29) Tian, W. D., Sage, J. T., Srajer, V., and Champion, P. M. (1992) Relaxation dynamics of myoglobin in solution. *Phys. Rev. Lett. 68*, 408−411.
(30) Heering, H. A., Smith, A. T., and Smulevich, G. (2002) Spectroscopic characterization of mutations at the Phe41 position in the distal haem pocket of horseradish peroxidase C: Structural and functional consequences. *Biochem. J. 363*, 571−579.
(31) Du, J., Huang, X., Sun, S., Wang, C., Lebioda, L., and Dawson, J. H. (2011) *Amphitrite ornata* Dehaloperoxidase (DHP): Investigations of Structural Factors That Influence the Mechanism of Halophenol Dehalogenation Using "Peroxidase-like" Myoglobin Mutants and "Myoglobin-like" DHP Mutants. *Biochemistry 50*, 8172−8180.
(32) Belyea, J., Gilvey, L. B., Davis, M. F., Godek, M., Sit, T. L., Lommel, S. A., and Franzen, S. (2005) Enzyme Function of the Globin Dehaloperoxidase from *Amphitrite ornate* Is Activated by Substrate Binding. *Biochemistry 44*, 15637−15644.
(33) Nelson, M. T., Humphrey, W., Gursoy, A., Dalke, A., Kale, L. V., Skeel, R. D., and Schulten, K. (1996) NAMD: A parallel, object oriented molecular dynamics program. *International Journal of Supercomputer Applications and High Performance Computing 10*, 251−268.
(34) Phillips, J. C., Braun, R., Wang, W., Gumbart, J., Tajkhorshid, E., Villa, E., Chipot, C., Skeel, R. D., Kale, L., and Schulten, K. (2005) Scalable molecular dynamics with NAMD. *J. Comput. Chem. 26*, 1781−1802.
(35) Humphrey, W., Dalke, A., and Schulten, K. (1996) VMD: Visual molecular dynamics. *J. Mol. Graphics 14*, 33−38.
(36) Otwinowski, Z., and Minor, W. (1997) Processing of X-ray diffraction data collected in oscillation mode. *Methods Enzymol. 276*, 307−326.
(37) McCoy, A. J., Grosse-Kunstleve, R. W., Adams, P. D., Winn, M. D., Storoni, L. C., and Read, R. J. (2007) Phaser crystallographic software. *J. Appl. Crystallogr. 40*, 658−674.
(38) Emsley, P., and Cowtan, K. (2004) Coot: Model-building tools for molecular graphics. *Acta Crystallogr. D60*, 2126−2132.
(39) Murshudov, G. N., Vagin, A. A., and Dodson, E. J. (1997) Refinement of macromolecular structures by the maximum-likelihood method. *Acta Crystallogr. D53*, 240−255.
(40) Franzen, S., Sasan, K., Sturgeon, B. E., Lyon, B. J., Battenburg, B. J., Gracz, H., Dumariah, R., and Ghiladi, R. (2012) Nonphotochemical Base-Catalyzed Hydroxylation of 2,6-Dichloroquinone by H_2O_2 Occurs by a Radical Mechanism. *J. Phys. Chem. B 116*, 1666−1676.
(41) Franzen, S., Belyea, J., Gilvey, L. B., Davis, M. F., Chaudhary, C. E., Sit, T. L., and Lommel, S. A. (2006) Proximal cavity, distal histidine and substrate hydrogen-bonding mutations modulate the activity of *Amphitrite ornata* dehaloperoxidase. *Biochemistry 45*, 9085−9094.
(42) Lente, G., and Espenson, J. H. (2004) Unusual Kinetic Role of a Water-Soluble Iron(III) Porphyrin Catalyst in the Oxidation of 2,4,6-Trichlorophenol by Hydrogen Peroxide. *Int. J. Chem. Kinet. 36*, 449−455.
(43) Nicoletti, F. P., Thompson, M. K., Howes, B. D., Franzen, S., and Smulevich, G. (2010) New Insights into the Role of Distal Histidine Flexibility in Ligand Stabilization of Dehaloperoxidase-Hemoglobin from *Amphitrite ornata*. *Biochemistry 49*, 1903−1912.

(44) Nicoletti, F. P., Thompson, M. K., Franzen, S., and Smulevich, G. (2011) Degradation of sulfide by dehaloperoxidase-hemoglobin from *Amphitrite ornata*. *JBIC, J. Biol. Inorg. Chem. 16*, 611−619.
(45) Belyea, J., Belyea, C. M., Lappi, S., and Franzen, S. (2006) Resonance Raman Study of Ferric Heme Adducts of Dehaloperoxidase from *Amphitrite ornata*. *Biochemistry 45*, 14275−14284.
(46) de Serrano, V. S., Davis, M. F., Gaff, J. F., Zhang, Q., Chen, Z., D'Antonio, E. L., Bowden, E. F., Rose, R., and Franzen, S. (2010) X-ray structure of the metcyano form of dehaloperoxidase from *Amphitrite ornata*: Evidence for photoreductive dissociation of the iron-cyanide bond. *Acta Crystallogr. D66*, 770−782.
(47) Laskowski, R. A. (1995) SURFNET: A program for visualizing molecular surfaces, cavities, and intermolecular interactions. *J. Mol. Graphics 13*, 307−308 , 323−330.